JOURNAL OF MATERIALS SCIENCE 32 (1997) 2771–2780

Mechanics of the maize leaf: a composite beam model of the midrib

B. MOULIA
Plant Biomechanics Group, U.R. de Bioclimatologie, INRA, 78850 Thiverval-Grignon, France

M. FOURNIER
Laboratoire de Rhéologie du Bois de Bordeaux, UMR 123 CNRS, INRA, Univ. Bdx I, B.P. 10, 33610 Cestas-Gazinet, France

The midrib is the major stiffening element of maize leaves. Its anatomical study reveals a complex cross-sectional shape and a composite constitutive material. A mechanical model is proposed, based on composite beam theory, to account for the bending mechanical behaviour of a beam element with an heterogeneous cross-section of any transverse shape. The inputs into the model are the outlines of the various material surfaces within the cross-section, and their corresponding Young's moduli. The predicted outputs are tested against experimental data from an *in vivo* flexural test. The model prediction gives a good first order approximation of the experimental data. The maize midrib can thus be considered as a sandwich beam. The model can also be applied more generally to any plant axis, once given the outlines and the rheologies of its constitutive material.

1. Introduction

This paper is part of a long-term research effort directed to understanding the mechanics and forms of grass leaves. Understanding the mechanics of such leaves can be of interest both for agronomists and for mechanical engineers, as leaves are a natural occurrence of composite structures [1–4]. In a previous study [5], an *in vivo* mechanical analysis of the flexural behaviour of the maize leaf allowed us to establish that the midrib (i) is morphologically a very slender structure (aspect ratio > 100) (ii) is the major stiffening element of the fully turgid maize leaf, and (iii) displays in most cases an elastic and locally linear behaviour. Such results lead naturally to an attempt to model the midrib within the framework of beam theory. In this paper, a composite beam model is thus proposed, which is a generalization of the previous works by Gibson *et al.* [2] and by Niklas [4]. It is shown that the mechanical behaviour of the midrib can be accounted for by the model, to at least a first approximation.

2. Geometry and micro-structure (anatomy) of the midrib cross-section

Fig. 1a shows the general morphology of the leaf in maize (*Zea mays* L.), and Fig. 1b details the outlines of three successive cross-sections along the maize midrib. The overall geometry of the cross-section is usually, at the base of the midrib, a thick U (or V) and then goes to a more rounded shape toward the tip of the leaf. However, both the longitudinal gradients of changes of cross-sectional shape and of tapering are small ($\approx 7 \times 10^{-3}$ for the gradient of the mean radius of cross-sectional area). Note finally that the midrib displays most of the time an approximate mirror symmetry apart from the vertical plane.

The internal micro-structure of the midrib is shown in Fig. 2a. It is obvious that at least two different materials can be distinguished. The core of the midrib is made of a foam-like cellular tissue of very low density. This tissue is called in botany a parenchyma. It has very large cells and extremely thin cell walls. The outer "rind" is made of a much denser material. A more magnified view using staining (safranin + blue astra) and polarized microscopy (Fig. 2b) shows that the rind itself is heterogeneous, being made of vascular bundles and of a very dense tissue with thick cell walls, called the sclerenchyma. However, both the bundles and the sclerenchyma are denser than the central parenchyma and they have a rather similar chemical composition of the cell wall (mainly sclerified tissues).

3. Mechanical model of the bending stiffness and suppleness

Models of leaves in which they are considered as sandwich beams in bending have already been proposed [2, 4]. However, such models are based on simple idealizations of the cross-sectional geometry (rectangular or circular cross-section), with a level of symmetry high enough to fix the position of the neutral fibre. On the other hand, unfortunately the maize midrib does not display a geometry that is amenable

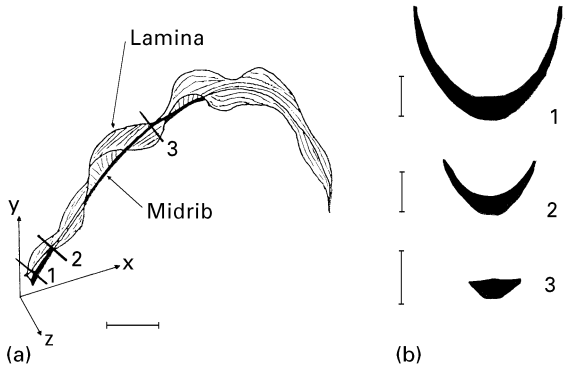

Figure 1 General morphology of the midrib of the maize leaf. (a) the midrib within the leaf (horizontal bar = approx. 10 cm) and (b) shadow-graphs of three successive cross-sections of the midrib (their initial situations within the midrib are shown in a) (vertical bars = 5 mm).

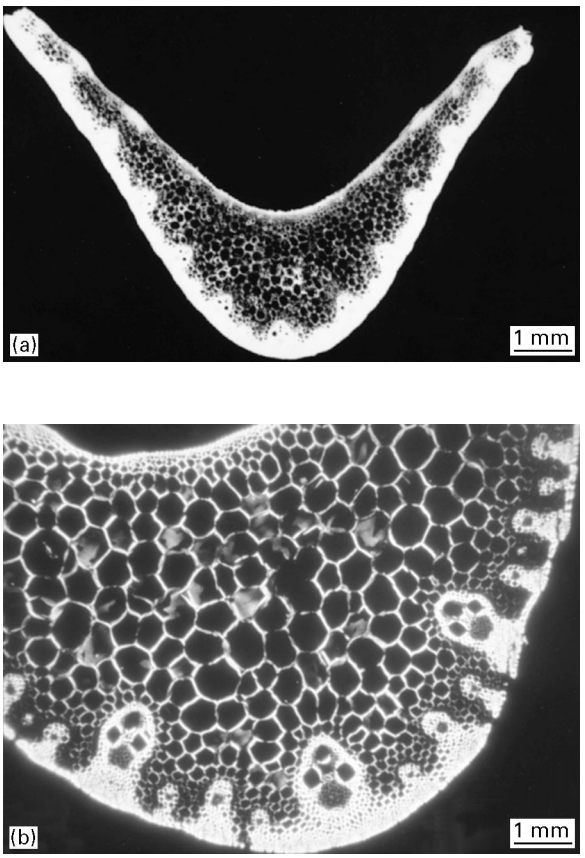

Figure 2 The anatomical microstructure of the midrib cross-section: (a) negative macrophotograph of the whole cross-section (b) more detailed view using safranin plus astra blue staining and polarized microscopy.

to an idealization with simple shapes (see Fig. 1). Moreover it has only (at best) a bilateral symmetry, so that the position of the neutral fibre (at least within the plane of symmetry) is an unknown quantity, which has to be determined by the mechanical model. The model developed in the following sections deals with the bending behaviour of an element of a beam with an heterogeneous cross-section, whatever the cross-sectional shape. The various materials within the

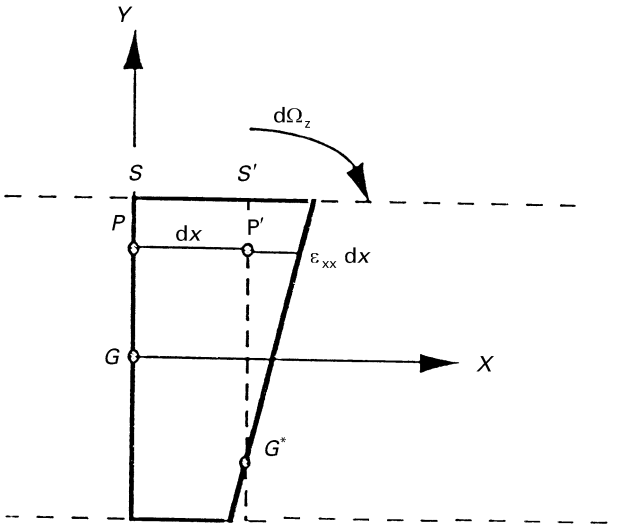

Figure 3 The parameterization of the longitudinal strain field according to the Navier–Bernouilli assumption: S and S' are two successive cross-sections dx apart, $d\Omega_Z$ rotation angle of the cross-section S', G centroid point of the cross-section, G^* neutral point of the cross-section.

cross-section are assumed to be distributed within distinct surfaces, defined by their outlines. It is thus a generalization of the previous models (still staying, however, within the framework of the theory of composite beams in pure bending [6] as no attempt is made to take into account shear, because of the highly slender nature of the midrib).

Consider a beam whose cross-section S includes n distinct material surfaces $D_i(i \in \{1, \ldots, n\})$, defined by their outlines and by the longitudinal Young's moduli of their material. The beam is assumed to be initially only slightly curved within a plane. The cross-section S is loaded by a bending moment $\hat{M}f$ (assumption of pure bending); the reference frame on S is $G\ XYZ$(G = centre of area of the cross-section, X = tangent to the central line, Y = vertical). Using the classical kinematical assumption of the beam theory, which states that the cross-section remains plane and perpendicular to the directing curve of the beam (Navier–Bernoulli's assumption), the longitudinal strain (along X) can be set as (see Fig. 3)

$$\varepsilon_{xx}(s)(y, z) = \varepsilon_0(s) - \left(\frac{d\Omega_z}{dx}(s)\, y\right) + \left(\frac{d\Omega_Y}{dx}(s) z\right) \tag{1}$$

where ε_{xx} is the longitudinal strain, s is the curvilinear abscissa of the cross-section S along the central line of the beam, ε_0 is the longitudinal strain on the central line, $d\Omega_z/dx$ is the lineic rotation angle of the cross-section around the Z axis and $d\Omega_Y/dx$ is the lineic rotation angle of the cross-section around the Y axis.

For the sake of clarity, Equation 1 can be modified into:

$$\varepsilon_{xx}(s)(y, z) = \varepsilon_0(s) - (\delta C_{XY}(s) y) + (\delta C_{XZ}(s) z) \tag{2}$$

where δC_{IJ} is the change in curvature of the projection of the central line of the beam within the plane IJ.

The constitutive law of any material i is taken as linear elastic. Considering only the components along

X, it can be shown that:

$$\sigma^{i}_{XX} = E^{i}_{L}\varepsilon_{XX} \tag{3}$$

where E^{i}_{L} is the apparent Young's modulus of the material i and σ^{i}_{XX} is the longitudinal stress in the material i.

Note that it is assumed that the constitutive materials if anisotropic, have one of their major directions of anisotropy concurrent with X, an assumption which seems to be realistic in the maize midrib (if not the case, the application of a bending moment would induce shear, resulting for example in a coupling between bending and torsion). Moreover, we choose to neglect the hardening of the apparent longitudinal stiffness due to putative non-compatibility of the transverse strains generated by Poisson's effects. As a matter of fact, these effects are usually of second order, notably in the case of anisotropic beams with the longitudinal direction being the stiffest [6, 7], as is the case in the maize midrib. Finally it should be noted that Equations 2 and 3 lead to a discontinuous field of longitudinal stress σ_{XX} (continuous by pieces).

The relations between the normal force N, the bending moments M_Y, M_Z and the longitudinal stress can be written as

$$N = \iint_S \sigma_{xx}\,dydz \tag{4}$$

$$M_Y = \iint_S (\sigma_{xx}z)\,dydz \tag{5}$$

$$M_Z = \iint_S (-\sigma_{xx}y)\,dydz \tag{6}$$

Substituting for σ_{xx} into Equations 4–6 from the constitutive law (Equation 3), and then substituting for ε_{XX} from Equation 2 yields:

$$\begin{cases} N = \sum_{i=1}^{n}\left[\iint_{D_i}(E^{i}_{L}(\varepsilon_0 - \delta C_{XY}\,y + \delta C_{XZ}\,z))\,dydz\right] & (7)\\ M_Y = \sum_{i=1}^{n}\left[\iint_{D_i}(E^{i}_{L}(\varepsilon_0 - \delta C_{XY}\,y + \delta C_{XZ}\,z)z)\,dydz\right] & (8)\\ M_Z = \sum_{i=1}^{n}\left[\iint_{D_i}(-E^{i}_{L}(\varepsilon_0 - \delta C_{XY}\,y + \delta C_{XZ}\,z)\,y)\,dydz\right] & (9)\end{cases}$$

which can be put in the form:

$$\Rightarrow\begin{cases} N = \sum_{i=1}^{n}\left[E^{i}_{L}\left(\varepsilon_0\left(\iint_{D_i}dydz\right) - \delta C_{XY}\left(\iint_{D_i}y\,dydz\right) + \delta C_{XZ}\left(\iint_{D_i}z\,dydz\right)\right)\right] & (10)\\ M_Y = \sum_{i=1}^{n}\left[E^{i}_{L}\left(\varepsilon_0\left(\iint_{D_i}z\,dydz\right) - \delta C_{XY}\left(\iint_{D_i}yz\,dydz\right) + \delta C_{XZ}\left(\iint_{D_i}z^2dydz\right)\right)\right] & (11)\\ M_Z = \sum_{i=1}^{n}\left[-E^{i}_{L}\left(\varepsilon_0\left(\iint_{D_i}y\,dydz\right) - \delta C_{XY}\left(\iint_{D_i}y^2\,dydz\right) + \delta C_{XZ}\left(\iint_{D_i}yz\,dydz\right)\right)\right] & (12)\end{cases}$$

and finally lead to the matrix equation

$$\begin{pmatrix} N\\ M_Y\\ M_Z\end{pmatrix} = \begin{pmatrix} \sum_{i=1}^{n}E^{i}_{L}A_i & \sum_{i=1}^{n}E^{i}_{L}A_i z_{Gi} & -\sum_{i=1}^{n}E^{i}_{L}A_i y_{Gi}\\ \sum_{i=1}^{n}E^{i}_{L}A_i z_{Gi} & \sum_{i=1}^{n}E^{i}_{L}I^{i}_{Y} & -\sum_{i=1}^{n}E^{i}_{L}I^{i}_{YZ}\\ -\sum_{i=1}^{n}E^{i}_{L}A_i y_{Gi} & -\sum_{i=1}^{n}E^{i}_{L}I^{i}_{YZ} & \sum_{i=1}^{n}E^{i}_{L}I^{i}_{Z}\end{pmatrix} \times \begin{pmatrix} \varepsilon_0\\ \delta C_{XZ}\\ \delta C_{XY}\end{pmatrix} \tag{13}$$

where A_i is the area of the material surface D_i, y_{Gi} is the Y-ordinate of the centre of area of the material surface D_i, z_{Gi} is the Z-ordinate of the centre of area of the material surface D_i, I_Y is the second moment of area relative to the axis GY, I_Z is the second moment of area relative to the axis GZ, I_{YZ} is the area product, relative to the axes GY, GZ,

$$A_i = \iint_{D_i}dydz,\ y_{Gi} = \frac{1}{A_i}\iint_{D_i}y\,dydz,\ z_{Gi} = \frac{1}{A_i}\iint_{D_i}z\,dydz,$$

$$I^{i}_{Y} = \iint_{D_i}z^2\,dydz,\ I^{i}_{Z} = \iint_{D_i}y^2\,dydz,\ I^{i}_{YZ} = \iint_{D_i}yz\,dydz$$

Note that Equation 13 represents the behaviour law of the beam element loaded by a combined tensile and bending load.

Introducing the hypothesis of pure bending leads to

$$\begin{aligned} N = 0 \Leftrightarrow{}& \varepsilon_0\left(\sum_{i=1}^{n}E^{i}_{L}A_i\right) - \delta C_{XY}\left(\sum_{i=1}^{n}E^{i}_{L}A_i y_{G_i}\right)\\ &+ \delta C_{XZ}\left(\sum_{i=1}^{n}E^{i}_{L}A_i z_{G_i}\right) = 0\\ \Leftrightarrow{}& \varepsilon_0 = \delta C_{XY}\left(\frac{\sum_{i=1}^{n}E^{i}_{L}A_i y_{G_i}}{\sum_{i=1}^{n}E^{i}_{L}A_i}\right)\\ &- \partial C_{XZ}\left(\frac{\sum_{i=1}^{n}E^{i}_{L}A_i z_{G_i}}{\sum_{i=1}^{n}E^{i}_{L}A_i}\right)\end{aligned} \tag{14}$$

let the point $G^*\begin{pmatrix} y_{G^*} \\ z_{G^*} \end{pmatrix}$

defined as:

$$\begin{cases} y_{G^*} = \dfrac{1}{\sum\limits_{i=1}^{n} E_L^i A_i} \sum\limits_{i=1}^{n} E_L^i A_i y_{Gi} \\ z_{G^*} = \dfrac{1}{\sum\limits_{i=1}^{n} E_L^i A_i} \sum\limits_{i=1}^{n} E_L^i A_i z_{Gi} \end{cases} \tag{15}$$

(i.e., as G^* is the barycentre of the centres of area of all the material surfaces in the cross-section, weighted by their longitudinal tensile stiffness)

Then Equation 14 can be modified as:

$$\varepsilon_0 = \delta C_{XY} y_{G^*} - \delta C_{XZ} z_{G^*} \tag{16}$$

Note that Equation (16) means that the straining of the central line of the beam is only a consequence of the rotation of the cross-section around G^*. Thus G^* is on the elastic neutral fibre, whose displacement from the central line of the beam is a function of the tensile stiffness and of the position of the materials within the cross-section.

Substituting for ε_0 in Equation 13 from Equation 16 yields:

$$\begin{cases} M_Y = -\delta C_{XY}\left(\sum\limits_{i=1}^{n} E_L^i (I_{YZ}^i - A_i y_{G^*} z_{G^*})\right) \\ \qquad + \delta C_{XZ}\left(\sum\limits_{i=1}^{n} E_L^i (I_Y^i - A_i z_{G^*}^2)\right) \\ M_Z = \delta C_{XY}\left(\sum\limits_{i=1}^{n} E_L^i (I_Z^i - A_i y_{G^*}^2)\right) \\ \qquad - \delta C_{XZ}\left(\sum\limits_{i=1}^{n} E_L^i (I_{YZ}^i - A_i y_{G^*} z_{G^*})\right) \end{cases} \tag{17}$$

It is better to translate the reference frame in G^*; after a little calculation (which is detailed in Appendix 2) it yields:

$$\begin{cases} M_Y = -\delta C_{XY}\left(\sum\limits_{i=1}^{n} (E_L^i I_{YZ}^{i*})\right) + \delta C_{XZ}\left(\sum\limits_{i=1}^{n} (E_L^i I_Y^{i*})\right) \\ M_Z = \delta C_{XY}\left(\sum\limits_{i=1}^{n} (E_L^i I_Z^{i*})\right) - \delta C_{XZ}\left(\sum\limits_{i=1}^{n} (E_L^i I_{YZ}^{i*})\right) \end{cases} \tag{18}$$

let then $K_Y^* = \sum\limits_{i=1}^{n} E_L^i I_Y^{i*}$, $K_Z^* = \sum\limits_{i=1}^{n} E_L^i I_Z^{i*}$, $K_{YZ}^* = \sum\limits_{i=1}^{n} E_L^i I_{YZ}^{i*}$

and substitute for them into Equation 18, yielding

$$\begin{pmatrix} M_Y \\ M_Z \end{pmatrix} = \begin{pmatrix} K_Y^* & -K_{XY}^* \\ -K_{XY}^* & K_Z^* \end{pmatrix} \begin{pmatrix} \delta C_{XZ} \\ \delta C_{XY} \end{pmatrix} \tag{19}$$

The 2nd order symmetric matrix $K_{m,n}$ represents the tensor of bending rigidity (associated with the beam element), in the reference frame G^*XYZ. This may be a matter of surprise as the bending moment M was initially defined on the axes GZ, GY and the change in curvature δC relative to the centre line of the beam. However M is unchanged by the translation from G to G^* as $N = 0$. δC can also be considered as unchanged, provided that the initial curvature of the beam is small (i.e., the radius of curvature is much greater than the thickness of the midrib, which is the case in the maize midrib [5]). Note also that there is a coupling of the bendings. For example if the only loading is $M_Z (M_Y = 0)$ the bending plane runs out of the vertical (skew bending).

It is then interesting to diagonalize the matrix $K_{m,n}$ in order to find the reference frame called the "principal axes of bending rigidity", in which there is no more coupling of the bendings. Let us define it in terms of G^*, Y_p and Z_p.

The eigenvalues of $K_{m,n}$ are:

$$K_p^* = \tfrac{1}{2}\left[(K_Y^* + K_Z^*) \pm ((K_Y^* - K_Z^*)^2 + 4(K_{YZ}^*)^2)^{1/2}\right] \tag{20}$$

and the eigenvectors (which define the directions of the principal axes $Y_p Z_p$) are:

$$\begin{pmatrix} \dfrac{K_{YZ}^*}{(K_Y^* - K_{Y_p}^*)} \dfrac{1}{\left(1 + \left(\dfrac{K_{YZ}^*}{K_Y^* - K_{Y_p}^*}\right)^2\right)^{1/2}} \\ \dfrac{1}{\left(1 + \dfrac{K_{YZ}^*}{K_Y^* - K_{Y_p}^*}\right)^2\Big)^{1/2}} \end{pmatrix}$$

$$\begin{pmatrix} \dfrac{-1}{\left(1 + \left(\dfrac{K_{YZ}^*)}{K_Y^* - K_{Y_p}^*}\right)^2\right)^{1/2}} \\ \dfrac{K_{YZ}^*}{(K_Y^* - K_{Y_p}^*)} \dfrac{1}{\left(1 + \left(\dfrac{K_{YZ}^*}{K_Y^* - K_{Y_p}^*}\right)^2\right)^{1/2}} \end{pmatrix} \tag{21}$$

Y_p^* and Z_p^* are chosen so that they make the direct reference frame so that $\langle \vec{Y}_p \cdot \vec{Y} \rangle$ is maximum. From the principal axes, it is also possible to calculate the polar "skew angle" φ^* between G^*Y and G^*Y_p, given that:

$$\tan(\varphi^*) = \frac{Z(\vec{Y}_p)}{Y(\vec{Y}_p)} = \frac{(K_Y^* - K_{Y_p}^*)}{K_{YZ}^*} \tag{22}$$

The principal axes of rigidity being defined, the matrix in (G^*, Y_p, Z_p) of the bending rigidity tensor is:

$$\underline{\underline{K}} = \begin{pmatrix} K_{Y_p}^* & 0 \\ 0 & K_{Z_p}^* \end{pmatrix} \tag{23}$$

Lastly, the matrix can be inverted, to obtain the principal matrix of the bending suppleness tensor:

$$\underline{\underline{S}} = \begin{pmatrix} S_{Y_p}^* & 0 \\ 0 & S_{Z_p}^* \end{pmatrix} = \begin{pmatrix} \dfrac{1}{K_{Y_p}^*} & 0 \\ 0 & \dfrac{1}{K_{Z_p}^*} \end{pmatrix}$$

$$= \begin{pmatrix} \dfrac{1}{\sum_{i=1}^{n} E_{\mathrm{L}}^{\mathrm{i}} I_{\mathrm{Y_p}}^{\mathrm{i}*}} & 0 \\ 0 & \dfrac{1}{\sum_{i=1}^{n} E_{\mathrm{L}}^{\mathrm{i}} I_{\mathrm{Z_p}}^{\mathrm{i}*}} \end{pmatrix} \quad (24)$$

These calculations have been coded in Turbo-Pascal on a personal computer, giving raise to a software package called RIGFLEX. The various moments of area are computed numerically from the outlines of the material surfaces within the cross-section, using the trapezia method. The inputs into the model are thus the outlines of all the material surfaces within the cross-section, and the longitudinal Young's moduli of the various materials. The outputs are all the moment of area, the matrices of bending rigidity in the usual axes and in the major axes, the matrix of suppleness, and the skew angle φ^*. A graphical display of the composite cross-section in the usual axes (for a checking of the inputs) and in the principal axes of rigidity is also implemented.

4. Qualification of the model inputs

4.1. Cross-sectional morphometrics

The plant material has been described by Moulia *et al.* [5] and the midribs used are those previously tested with the *in vivo* bending test [5]. Freehand anatomical transverses sections were done on fresh material, without any special treatment. The curvilinear abscissa of each section along the midrib was recorded. Ten midribs were studied, with a mean of 13 sections per midrib (in order to describe the tapering and the changes in cross-sectional shape of the midrib). The leaves were of two ranks along the stem (rank 8 and 10). In order to minimize the changes in volume due to cell disruption and to desiccation, the cuts were made rather thick (≈ 1 mm) and immediately placed in a drop of pure water, on a graduated glass lamella. A negative macrophotograph (similar to the one shown Fig. 2a) was obtained by mounting the glass lamella with the specimen on a photographic enlarger. Care was taken to place the cross-section in the same orientation within the YZ plane as observed *in situ* within the midrib. A magnified negative photograph was then printed by transmission on a photosensitive paper that was immediately developed. The difference in optical density from the inner core and the outer ring is related to density differences and also to the chlorophyll that is concentrated in some cells of the outer ring. More detailed anatomical studies using several staining techniques (safranin plus astra blue, chlorhydric phloroglucinol and Maüle's reactive) revealed that the transmission photograph induces an homogenization of the outer rind but that its outlines were generally correct. The outlines of the material areas were then digitized from the photograph as set of points using a 2D digitizing tablet (Summasketch Pro, Summagraphics Corp., Seymour, CO, USA, 0.01 mm accuracy). The accuracy of the morphometrics measurements can be split into two effects: (i) the accuracy on the measurement of the scale magnification among photographs and (i) the accuracy on the digitizing of the outlines. The coefficient of variation on the first type of error is 0.3% ($n = 30$). For the second type of error, the coefficient of variation is 1% on the estimate of the cross-sectional area and less than 3.5% for the estimate of the principal bending rigidity (see section 2 for details on the choice of the rheological constants).

4.2. Longitudinal Young's moduli

No attempt has been made directly to measure the Young's moduli of the parenchyma and of the rind tissue(s). We decided, as a first approach, to rely on the literature data. Our goal is then to test whether a composite model taking into account the longitudinal changes in cross-sectional geometry (including the geometry of the various material domains) is sufficient to explain the bending stiffness. As a matter of fact, previous experimental studies on plant slender organs indicate that changes in geometry along the plant axis are much more important for the bending rigidity than changes in the "homogenized equivalent Young modulus" of the cross-section. Moreover, no obvious anatomical change is observed along the midrib, and our composite modelling takes into account most of the changes in the "homogenized equivalent Young modulus" of the cross-section, by including the effects of possible changes in the volumetric fractions of core and rind tissues.

Tables I and II summarize the literature data, concerning the parenchyma and the sclerified tissues. The order of magnitude of the Young's moduli is around 10^2 MPa for the leaf parenchyma. For the sclerified tissues it ranges from 10^2 MPa for vascular bundles to 10^4 MPa for sclerenchyma, being close to 10^3 MPa for leaf heterogeneous sclerified tissues. Note that in all cases the variability of the measurements is high. From these results, we have decided to distinguish only two materials within the cross-section (parenchymatous core and sclerified rind) and to value their Young's moduli respectively as $E_c = 10^2$ MPa and $E_r = 10^3$ MPa. It should be also noted that retaining these values to test the model against experimental data adds two restrictive and non-mechanical hypotheses to the model. It is assumed that the constitutive law of the parenchyma and sclerified tissues do not change (i) across a given section and (ii) along the midrib. When these two assumptions are added to our model of the mechanical behaviour of the composite beam element we will speak, to be short, of the simplified model.

5. Comparison between the simplified model and the experimental data

5.1. Skew angle of the cross-section

Before testing the results of the model against the experimental data, it is necessary to recall that the experimental data were obtained under the assumption of pure plane bending. It is thus interesting to check whether the results from the model are in

TABLE I Longitudinal Young's moduli of sclerified tissues from herbaceous plants

Tissue	Organ *Species*	Type test	Size of the specimen (mm)	Strain rate	Water status	E_L (MPa) ($\pm$std%.)	Notes	References
Sclerified tissues (sclerenchyma + vascular bundles + parenchymatous sheath)	Stem *Zea mays* L.	Tensile	$20 \times 5 \times 1$	0.1 mn^{-1}	Wet	**10^3 à 10^4**	(30 specimens) The major source of variance is the radial position within the stem	[8]
Sclerified tissues (sclérenchyma + chlorenchyma)	Leaf *Juncus effusus* L.	MFRS*			Wet	**2.3 10^3** ($\pm$ 22%)		[4]
Sclerified tissues (sclérenchyma + + vascular bundles	Leaf *Iris* sp.	"Tensile"**	16×48 $\times 0.6$ to 3		Wet	**3.5 10^3**		[2]
Sclerenchyma	Leaf *Holcus lanatus*	Tensile		(50 mm. mn^{-1})	Wet	**3.0 10^3** ($\pm$ 63%)	(7 specimens)	[9]
Sclerenchyma	Leaf *Dactylis glomerata*	Tensile		(50 mm. mn^{-1})	Wet	**7.4 10^3** ($\pm$ 98%)	(8 specimens)	[9]
Sclerenchyma	Leaf *Bromis hordescens*	Tensile		(50 mm. mn^{-1})	Wet	**7.5 10^3** ($\pm$ 48%)	(9 specimens)	[9]
Sclerenchyma	Leaf *Deschampsia caespitosa*	Tensile		(50 mm. mn^{-1})	Wet	**3.6 10^3** ($\pm$ 59%)	(7 specimens)	[9]
Sclerenchyma	Leaf *Stipa gigantea*	Tensile		(50 mm. mn^{-1})	Wet	**2.1 10^3** ($\pm$ 46%)	(6 specimens)	[9]
Sclerenchyma	Leaf *Lolium perenne* L.	Tensile		(50 mm. mn^{-1})	Wet	**2.3 10^4** ($\pm$ 41%)	(7 specimens)	[1]
Sclerenchyma	Leaf ? ?				dry	**0.5 à 3.5 10^4**		[10]
Vascular bundles	Leaf *Lolium perenne* L.	Tensile		(50 mm. mn^{-1})	Wet	**8.4 10^2** ($\pm$ 55%)	(5 specimens)	[1]

* MFRS = dynamic test (Multiple resonance frequency spectra see [11]).
** In this work, the equivalent tensile Young's moduli E_{eq} of the whole cross section was measured, and the Young's moduli of each tissue was then calculated using their areas and their density.

TABLE II Young's moduli of leaf parenchyma

Tissue	Organ *Species*	Type test	Size of the specimens (mm)	Strain rate	Water status (w = water content)	E_L (MPa) ($\pm$std%.)	Notes	References
Aerenchyma	Leaf *Juncus effusus* L.	MFRS*			wet (soaked in pure water)	**3 10^2** ($\pm$ 33%)		[4]
Parenchyma	Leaf *Iris* sp.	"Tensile"**	16 × 48 × 0.6 à3		wet (w $\approx$ 600%)	**2.1 10^2**		[2]

* MFRS = dynamic test (Multiple resonance frequency spectra see [11]).
** In this work, the equivalent tensile Young's moduli E_{eq} of the whole cross section was measured, and the Young's moduli of each tissue was then calculated using their areas and their density.

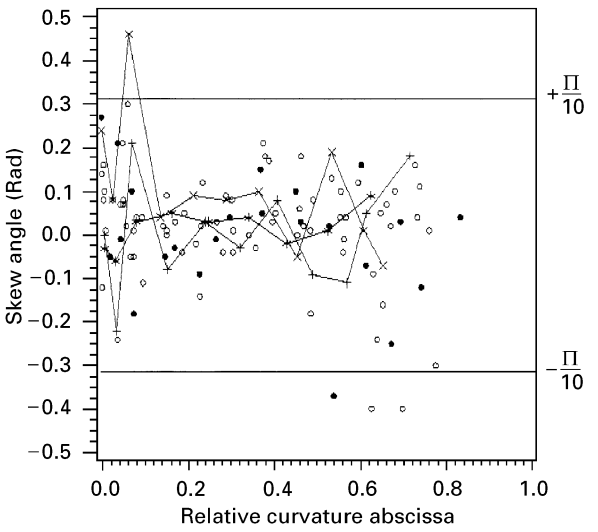

Figure 4 Calculated skew angles φ* for all the cross-sections (each point represents a cross-section, the lines are drawn only to identify the sets of cross-sections that are used latter to test the predictive power of the model) (●) rank 8, (○) rank 10, (+ --- +) leaf e20, rank 8, (× --- ×) leaf e22, rank 8, (∗——∗) leaf f22, rank 10.

TABLE III Mean skew angles of the cross sections sorted by leaf rank

Sample	Mean skew angle (Rad) $\pm$ stdev	Prob > |T| (Hyp mean = 0)
Midribs rank 8	+ 2.5 10^{-2} ($\pm$ 0.146)	0.24 NS
Midribs rank 10	+ 1.5 10^{-2} ($\pm$ 0.120)	0.25 NS

accordance with this assumption. Fig. 4 represents the skew angles φ* obtained by running the model on the morphometrical data from the cross-sections. The skew angles are very small and their mean are statistically not significantly different from zero (see Table III). These results quantitatively corroborate the previous observation of the bilateral symmetry of the midrib, and thus, the assumption of plane bending.

5.2. Validity of the outputs of the simplified model

In our previous experimental work [5], a considerable number of *in vivo* tests had to be discarded to obtain a good accuracy in the computation of changes in the curvature. From the 10 midribs described and modelled in the present work, only 3 provided reliable experimental data. However, as both the measured and the modelled supplenesses are local variables (along the midrib), this testing sample includes 23 anatomical sections (on which the model was run) and 126 experimentally measured points. Fig. 5(a–c) show the compared results obtained for the three leaves. The simplified model globally correctly accounts for the orders of magnitudes of the suppleness However, at least in two midribs (b, c), the changes in suppleness along the midrib are not correctly simulated. The model does not account for a rather sharp change in the slopes at curvilinear abscissa 200 and 300 mm. Several possible reasons can be put forward to explain such a discrepancy. The first reason may be that the assumption of homogeneity of the materials along the midrib is not correct in all the leaves. This could be for two reasons. The first one is some intrinsic changes in the stiffness of the materials, an hypothesis which can be tested only by investigating the rheologies of the constitutive materials. A second possibility is that some longitudinal changes occur in the fraction of vascular bundles within the rind. As these bundles are less dense than the sclerenchyma, this may induce changes in the rigidity of the composite beam. We have tested this hypothesis by again running the model considering 3 material areas (parenchyma, "sclerenchymal rind" and vascular bundles). Moreover, to emphasise the effect, we have set the Young's modulus of the bundles as equal to that of the parenchyma (10^2 MPa). The results are shown in Fig. 5(a and b) (that is on both a leaf with, and a leaf without, an unexplained change in slopes). It is clear that the change in slope cannot be explained by a bundle fraction effect.

The other reason which could induce the discrepancies between the model and the experiment along the midrib concerns the mechanical model itself. It may be first thought that it may not be correct to assume that the effect of the transverse shearing force can be neglected, even in such a slender structure. Owing to the distribution of shear stress within the cross-section, the shearing deflections should be increased in core–rind beams with a large core having a low shear modulus [12]. However, this cannot explain the observed differences. The shear deformations, if important, should lead to an over-estimation of the "bending suppleness" in the experiments (as they were analysed in pure bending [5]). Moreover, since (i) the bending moment is almost a linear function of the

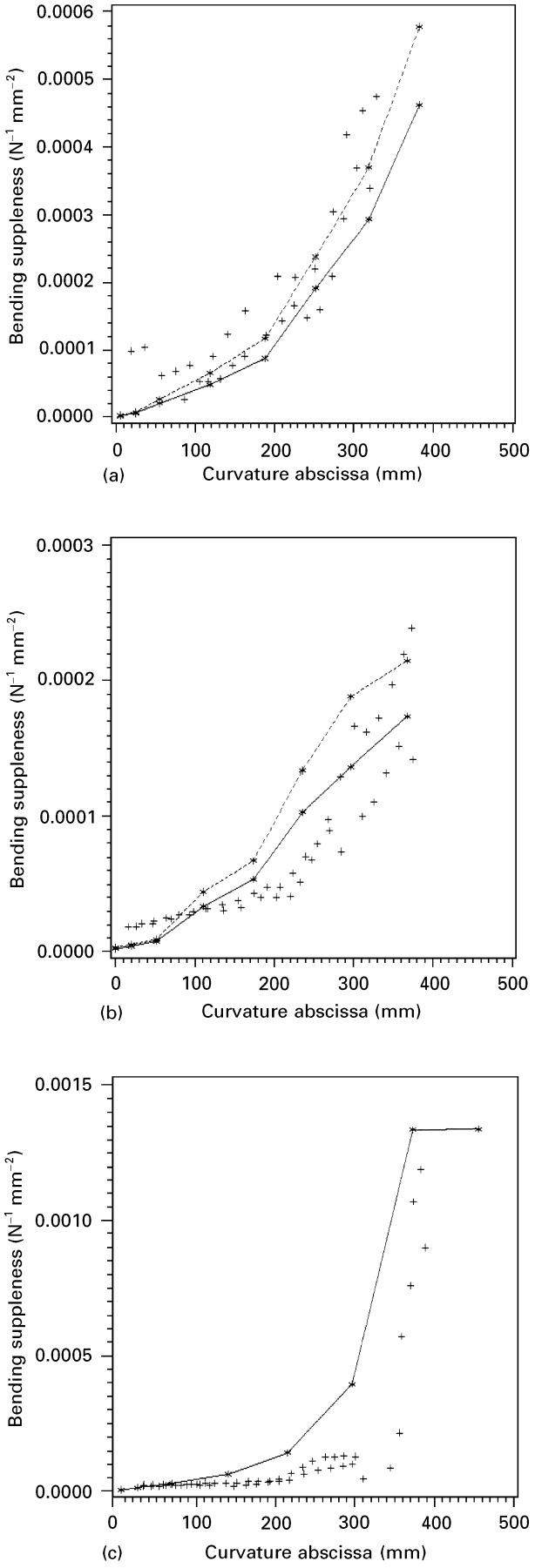

Figure 5 Experimental and simulated bending suppleness for three midribs (a) leaf e20, rank 8, (b) leaf e22, rank 8, (c) leaf f22, rank 10.: (+) measured suppleness, (∗——∗) simplified core-rind model ($E_c = 10^2$ MPa, $E_r = 10^3$ MPa), (∗– –∗) simplified core-bundles-sclerenchyma model ($E_c = E_b = 10^2$ MPa, $E_S = 10^3$ MPa).

curvilinear abscissa [5] and hence the transverse shear force is constant, and (ii) the area of the cross-section decreases linearly while the relative area of constitutive tissues remains constant [13], it follows that the effect of shearing can only explain a monotonically increasing difference between the model and the so called measured suppleness. This is not the case in this work.

The last possible reason for differences between experiments and the model is related to structural effects. A common characteristic of the midribs b and c (Fig. 5) is that their longitudinal initial habit showed a zone with sharper curvature which is located at the point where the change in slopes of the suppleness happens. It is possible that a structural coupling of the longitudinal and transverse curvatures occurs on these zones. leading to a decrease in the local apparent longitudinal bending rigidity [17]. Modelling such a behaviour, however, would require the abandonment of beam theory and the development of a 3D model.

6. Conclusion

The presented results show that the *in vivo* bending behaviour of the maize midrib can be accounted for by a composite beam model, at least to a first order approximation. This corroborates previous reports in the literature [2, 4, 12] stating that many herbaceous plant axes behave as sandwich beams. It is interesting to observe that 95% of the bending stiffness is provided by the sclerified rind, which represents less than 40% of the cross-sectional area of the beam. These results illustrate the interest in considering natural structures with the eyes of a mechanical engineer. A next step would be to compare different designs, in terms of cross-sectional shapes, and material distribution, and to investigate their different mechanical behaviour, their functional advantages and drawbacks. Our model should be highly suitable for such a study, as it is not only related to the cross-sectional shapes that are similar to those used in artificial designs. Note that it could rather easily be extended to the calculation of the torsional rigidity, which seems to also be of ecological significance [9, 10]. Another point which is interesting to elucidate is the behaviour of plant organs submitted to water depletion as current observation together with rheological data indicates changes in the mechanical behaviour [12, 13, 16]. This latter subsect is investigated in another publication [17].

Acknowledgements

We acknowledge Mr Arthaud, a plant anatomist at the E.N.I.T.A Bordeaux, for the original suggestion of using a photographic enlarger to obtain negative transmission views, and for the use of its anatomy laboratory. We also thank Olivia Delavaud, LMGC Montpellier and B. Chanson, LRBB, for the microscopic views using a polarizing microscope. We also thank B. Chauvin for his very useful technical support. The present work forms part of the thesis of B. Moulia, who received a grant from the Département

de Bioclimatologie, Institut National de la Recherche Agronomique (France).

Appendix 1 Definitions of the main biological terms used

Midrib: a central, thickened and more or less "V shaped" ridge (rib) within the leaf.

Turgid: a plant organ is said to be turgid when the hydrostatic pressure inside its living cells is positive. Such pressure (called the turgor pressure) is explained by the elastic reaction of the cell wall to volumetric strains related to water flowing into the cell. Such water flow is driven by osmotic differences between the cell content and the surrounding solution, and it stops when the turgor pressure equilibrates the osmotic one. "Fully turgid" means that turgor pressure is maximal.

Sclerified tissues: The cell wall of the cells of sclerified tissues is thick and highly lignified. As a consequence, the cells are no longer living (and thus have no internal turgor pressure).

Leaf rank: the number of the leaf within the sequence of leaf emergence (the first leaf to emerge has rank one).

Appendix 2 Detail of the calculation of the effect of moving the reference frame to G^*

Equation 17 relating the bending moments to the curvatures of the central line is (in the reference frame $GXYZ$)

$$\begin{cases} M_Y = -\delta C_{XY}\left(\sum_{i=1}^{n} E_L^i (I_{YZ}^i - A_i y_{G^*} z_{G^*})\right) \\ \qquad + \delta C_{XZ}\left(\sum_{i=1}^{n} E_L^i (I_Y^i - A_i z_{G^*}^2)\right) \\ M_Z = \delta C_{XY}\left(\sum_{i=1}^{n} E_L^i (I_Z^i - A_i y_{G^*}^2)\right) \\ \qquad - \delta C_{XZ}\left(\sum_{i=1}^{n} E_L^i (I_{YZ}^i - A_i y_{G^*} z_{G^*})\right) \end{cases} \quad \text{(A1)}$$

Note that:

$$\sum_{i=1}^{n} E_L^i (I_Z^i - y_{G^*}^2 A_i) = \sum_{i=1}^{n} E_L^i I_Y^i - 2y_{G^*}^2 \times \sum_{i=1}^{n} E_L^i A_i + y_{G^*}^2 \sum_{i=1}^{n} E_L^i A_i \quad \text{(A2)}$$

and that Equation 15 can be rewritten as:

$$y_{G^*} \sum_{i=1}^{n} E_L^i A_i = \sum_{i=1}^{n} E_L^i A_i y_{Gi} \quad \text{(A3)}$$

substituting Equation A3 into Equation A2 yields:

$$\begin{aligned} &\sum_{i=1}^{n} E_L^i (I_Z^i - y_{G^*}^2 A_i) \\ &\quad = \sum_{i=1}^{n} E_L^i I_Z^i - 2y_{G^*} \times \sum_{i=1}^{n} E_L^i A_i y_{Gi} + y_{G^*}^2 \times \sum_{i=1}^{n} E_L^i A_i \\ &\quad = \sum_{i=1}^{n} E_L^i (I_Z^i - 2y_{G^*} A_i y_{Gi} + A_i y_{G^*}^2 \\ &\quad = \sum_{i=1}^{n} E_L^i \left(\int\int_{D_i} y^2 \, dy \, dz - 2y_{G^*} \times \int\int_{D_i} y \, dy \, dz + \int\int_{D_i} y_{G^*}^2 \, dy \, dz \right) \\ &\quad = \sum_{i=1}^{n} \left(E_L^i \int\int_{D_i} (y - y_{G^*})^2 \, dy \, dz \right) \end{aligned} \quad \text{(A4)}$$

Then, noting that $\int\int_{D_i} (y - y_{G^*})^2 \, dy \, dz = I_Z^{i*}$ is the second moment of area of the material surface i relatively to the axis G^*Z Equation A4 yields:

$$\sum_{i=1}^{n} E_L^i (I_Z^i - y_{G^*}^2 A_i) = \sum_{i=1}^{n} E_L^i I_Z^{i*} \quad \text{(A5)}$$

By a similar calculation, it can be demonstrated that

$$\sum_{i=1}^{n} E_L^i (I_Y^i - z_{G^*}^2 A_i) = \sum_{i=1}^{n} E_L^i I_Y^{i*} \quad \text{(A6)}$$

$$\sum_{i=1}^{n} E_L^i (I_{YZ}^i - y_{G^*} z_{G^*} A_i) = \sum_{i=1}^{n} E_L^i I_{YZ}^{i*} \quad \text{(A7)}$$

where $\int\int_{D_i} (z - z_{G^*})^2 \, dy \, dz = I_I^{i*}$ is the second moment of area of the material surface i relatively to the axis G^*Y, $\int\int_{D_i} (y - y_{G^*})(z - z_{G^*}) \, dy \, dz = I_{YZ}^{i*}$ is the product of area of the material surface i relatively to the axes G^*Y, G^*Z.

It is thus possible, from Equations A5–A7 to obtain Equation 18

$$\begin{cases} M_Y = -\delta C_{XY}\left(\sum_{i=1}^{n} (E_L^i I_{YZ}^{i*})\right) + \delta C_{XZ}\left(\sum_{i=1}^{n} (E_L^i I_Y^{i*})\right) \\ M_Z = \delta C_{XY}\left(\sum_{i=1}^{n} (E_L^i I_Z^{i*})\right) - \delta C_{XZ}\left(\sum_{i=1}^{n} (E_L^i I_{YZ}^{i*})\right) \end{cases} \quad \text{(A8)}$$

References

1. J. F. V. VINCENT, *J. Mater. Sci.* **17** (1982) 856.
2. L. J. GIBSON, M. F. ASHBY and K. E. EASTERLING, *ibid.* **23** (1988) 3041.
3. A. J. GREENBERG, A. MEHLING, M. LEE and J. H. BOCK, *ibid.* **24** (1989) 2549.
4. K. NIKLAS, *Amer. J. Bot.* **78** (1991) 561.
5. B. MOULIA, M. FOURNIER and D. GUITARD, *J. Mater. Sci.* **29** (1994) 2359.
6. S. LAROZE and J. J. BARRAU, in "Mécanique des structures. Tome 3: Calcul des structures en matériaux composites" (Eyrolles, Masson, Paris, 1987).
7. M. FOURNIER, Thèse de Doctorat, INPL, Nancy (1989).
8. D. C. FOLEY, *Iowa State J. Res.* **58** (1983) 235.
9. J. F. V. VINCENT, *J. Mater. Sci.* **26** (1991) 1947.
10. R. D. PRESTON in "The physical biology of the plant cell walls" (Chapman and Hall, London, 1974).

11. K. J. NIKLAS and F. C. MOON, *Amer. J. Bot.* **75** (1988) 1517.
12. K. J. NIKLAS, in "Plant biomechanics: an engineering approach to plant form and function" (The University of Chicago Press, Chicago, 1992) p. 173.
13. B. MOULIA, Thèse de Doctorat, Univ. Bordeaux I, Bordeaux (1993).
14. S. VOGEL, *J. Exp. Bot.* **43** (1992) 1527.
15. A. R. ENNOS, *Ann. Bot.* **72** (1993) 123.
16. K. J. NIKLAS and T. D. O'ROURKE, *Amer. J. Bot.* **74** (1987) 1033.

Received 27 April 1994
and accepted 7 November 1995